PNAS RESEARCH ARTICLE | ASTRONOMY

# Electron heating in kinetic-Alfvén-wave turbulence

Muni Zhou[a,b,c,1], Zhuo Liu[a], and Nuno F. Loureiro[a]

Edited by Daniela Calzetti, University of Massachusetts Amherst, Amherst, MA; received December 11, 2022; accepted April 23, 2023

**We report analytical and numerical investigations of subion-scale turbulence in low-beta plasmas using a rigorous reduced kinetic model. We show that efficient electron heating occurs and is primarily due to Landau damping of kinetic Alfvén waves, as opposed to Ohmic dissipation. This collisionless damping is facilitated by the local weakening of advective nonlinearities and the ensuing unimpeded phase mixing near intermittent current sheets, where free energy concentrates. The linearly damped energy of electromagnetic fluctuations at each scale explains the steepening of their energy spectrum with respect to a fluid model where such damping is excluded (i.e., a model that imposes an isothermal electron closure). The use of a Hermite polynomial representation to express the velocity-space dependence of the electron distribution function enables us to obtain an analytical, lowest-order solution for the Hermite moments of the distribution, which is borne out by numerical simulations.**

plasma turbulence | electron heating | solar wind | Landau damping | kinetic Alfven waves

## Significance

Space and astrophysical plasmas exist in a turbulent state. Because collisions tend to be relatively rare, such plasmas are not readily amenable to a fluid-like description, and therefore, one cannot a priori expect that fluid-inspired turbulence phenomenology should apply to them. Indeed, this paper demonstrates the essential role of intrinsically kinetic effects in turbulent dynamics at scales below the ion Larmor radius and the coupled nature of physical processes happening in real and velocity spaces. Our prediction of the direct connection between intense current structures, Landau damping, and electron heating, as well as of remarkable properties of the electron distribution function, provides important insights for interpreting recent high-resolution in situ solar-wind measurements from satellites.

Plasma turbulence is ubiquitous in space and astrophysical systems as diverse as the Earth's magnetosphere (1), the solar wind (2, 3), the solar corona (4), accretion disks (5), and the interstellar and intracluster media (6). Many of these environments are sufficiently dilute that particle collisions are rare on the dynamical timescales of interest. As such, kinetic plasma descriptions are needed to understand turbulence in those environments. Despite decades of intensive research, formulating a predictive theoretical framework for the dynamics of turbulence in the phase space of positions and velocities has been a notoriously difficult problem, especially in the subion-scale range (the kinetic range), where various microphysical plasma processes are dynamically important.

Recent high-resolution, in situ measurements of electromagnetic fluctuations and plasma distribution functions from satellites such as the Magnetospheric Multiscale mission, *Cluster*, and the Parker Solar Probe have provided unprecedented opportunities to study the rich plasma dynamics in the subion range of the turbulence (7–11). One of the ultimate goals of these studies is to understand how energy is dissipated in weakly collisional plasmas and how the electrons and ions are energized (12). Answering these questions requires a comprehensive understanding of the phase-space dynamics of kinetic plasma turbulence.

In a collisional plasma, energy can only be thermalized through the "fluid channel," in which energy cascades to small spatial scales through nonlinear advection and finally dissipates by viscosity and resistivity (13–17), while the particle distribution remains close to local thermodynamic equilibrium (18). In a weakly collisional plasma, however, both particle free streaming along magnetic field lines and drifting with different gyroaveraged $\boldsymbol{E} \times \boldsymbol{B}$ velocities drive the "phase-mixing" process (e.g., refs. 19–21), which smooths out the electromagnetic fluctuations and develops complex structures in velocity space. This kinetic effect enables an additional "kinetic channel" for dissipation, in which energy transfers to small scales in velocity space (i.e., high velocity moments of the distribution function) and dissipates through collisions (21–25). Energy dissipation in kinetic turbulence occurs via a combination of these two channels—their relative importance being determined by the complex phase-space dynamics of kinetic turbulence (26–29), elucidating which is the main focus of this paper.

The kinetic dissipation channel is, in principle, susceptible to the *plasma echo* effect (30, 31), whereby free energy inverse cascades in velocity space, returning from the high to the low moments of the distribution function (i.e., phase unmixing). The occurrence of a collection of stochastic plasma echoes can cause kinetic turbulence to resemble fluid turbulence, in the sense that the only allowed energy-cascade channel in that case is the fluid-type cascade toward smaller spatial scales (26, 27). The significance of this effect has been confirmed by numerical simulations of collisionless plasma turbulence at scales above the ion Larmor radius ($\rho_i$) with isothermal electrons focusing on compressive fluctuations (32) and below $\rho_i$ with an electrostatic drift-kinetic model (33). However,

Author affiliations: [a]Plasma Science and Fusion Center, Massachusetts Institute of Technology, Cambridge, MA 02139; [b]Department of Astrophysical Sciences, Princeton University, Princeton, NJ 08544; and [c]School of Natural Science, Institute for Advanced Study, Princeton, NJ 08544

Author contributions: M.Z., Z.L., and N.F.L. designed research; performed research; contributed new reagents/analytic tools; analyzed data; and wrote the paper.

The authors declare no conflict of interest.

This article is a PNAS Direct Submission.



[1]To whom correspondence may be addressed. Email: munizhou@princeton.edu

This article contains supporting information online at https://www.pnas.org/lookup/suppl/doi:10.1073/pnas.2220927120/-/DCSupplemental.

Published May 30, 2023.

how the possible occurrence of plasma echoes can be reconciled with observations of efficient electron and ion heating (e.g., refs. 11 and 25) at kinetic scales is an open question.

In this work, we address the critical question of how electron heating occurs in sub-$\rho_i$ turbulence in the limit where the plasma pressure is small compared to the magnetic pressure (i.e., low plasma $\beta$). In the following sections, we describe the theoretical framework adopted in this work and derive a (nonlinear) lowest-order solution of the electron distribution function in velocity space, which we then show is supported by our numerical simulations. Our study shows that a self-consistent answer to the question of electron heating lies in the entwined nature of turbulent plasma dynamics in position and velocity space.

## Theoretical Framework

We adopt the simplest analytical framework that includes the key physical processes involved in this problem, known as the Kinetic Reduced Electron Heating Model (KREHM) (34). KREHM is a rigorous asymptotic reduction of gyrokinetics valid in the limit of low electron plasma-beta, $\beta_e \sim m_e/m_i$, with $\beta_e \equiv 8\pi n_{0e} T_{0e}/B_0^2$, where $B_0$ is the background magnetic (guide) field strength (assumed constant and directed along $\hat{\boldsymbol{z}}$), and $n_{0e}$ and $T_{0e}$ are the background electron density and temperature, respectively; $m_e$ and $m_i$ denote the electron and ion masses. Within this limit, the parallel streaming and electromagnetic effects are ordered out in the ion gyrokinetic equation. It follows that the ion flow velocity parallel to the background field is $u_{zi} = 0$, and ions become isothermal and electrostatic. Ion finite Larmor radius (FLR) effects are retained in the gyrokinetic Poisson's law,

$$\frac{\delta n_e}{n_{0e}} = \frac{1}{\tau}(\hat{\Gamma}_0 - 1)\frac{e\varphi}{T_{0e}}, \qquad [1]$$

where $\varphi$ is the electrostatic potential, $\delta n_e/n_{0e}$ is the electron density perturbation normalized to its background value, $\tau \equiv T_{0i}/T_{0e}$ is the background temperature ratio, and $\hat{\Gamma}_0$ is a gyroaveraging operator that has the closed-form expression $\Gamma_0(\alpha) = I_0(\alpha)e^{-\alpha}$ in Fourier space; here, $I_0$ is the zeroth-order modified Bessel function of the first kind and $\alpha = k_\perp^2\rho_i^2/2$, where $\rho_i = v_{\mathrm{th}i}/\Omega_i$ is the ion Larmor radius, $v_{\mathrm{th}i} = \sqrt{2T_{0i}/m_i}$ is the ion thermal velocity, and $\Omega_i = eB_0/m_i c$ is the ion Larmor frequency (we consider single charge ions in this work, $Z = 1$).

The electrons are described by a perturbed distribution function which, to order $\sqrt{m_e/m_i} \sim \sqrt{\beta_e}$ in the gyrokinetic expansion, can be written as $\delta f_e = g_e + (\delta n_e/n_{0e} + 2v_z u_{ze}/v_{\mathrm{th}e}^2)F_{0e}$, where $F_{0e}(|\boldsymbol{v}|) \equiv n_{0e}/(\sqrt{2\pi}v_{\mathrm{th}e})^3 \exp(-|\boldsymbol{v}|^2/2v_{\mathrm{th}e}^2)$ is the equilibrium Maxwellian defined with the mean electron temperature $T_{0e}$ and its corresponding thermal speed $v_{\mathrm{th}e} = \sqrt{2T_{0e}/m_e}$, and $\delta n_e$ and $u_{ze}$ (electron flow parallel to the guide field) are the zeroth and first moments of $\delta f_e$, respectively. Since $u_{zi} = 0$, the parallel component of Ampère's law, $J_z = -(c/4\pi)\nabla_\perp^2 A_z$, where $A_z$ is the parallel component of the vector potential, leads to $u_{ze} = (e/cm_e)d_e^2\nabla_\perp^2 A_z$, where $d_e = c/\omega_{pe}$ is the electron skin depth. Information about the second and higher moments of $\delta f_e$ is contained in the (reduced) distribution function $g_e$.

The dynamics of this system are described by fluid equations for the first two moments, coupled to a drift-kinetic equation for $g_e$:

$$\frac{1}{n_{0e}}\frac{d\delta n_e}{dt} = -\hat{\boldsymbol{b}}\cdot\boldsymbol{\nabla}\frac{e}{cm_e}d_e^2\nabla_\perp^2 A_z, \qquad [2]$$

$$\frac{d}{dt}(A_z - d_e^2\nabla_\perp^2 A_z) = -c\frac{\partial\varphi}{\partial z} + \frac{cT_{e0}}{e}\hat{\boldsymbol{b}}\cdot\boldsymbol{\nabla}\left(\frac{\delta n_e}{n_{0e}} + \frac{\delta T_{ze}}{T_{0e}}\right), \qquad [3]$$

$$\frac{dg_e}{dt} + v_z\hat{\boldsymbol{b}}\cdot\boldsymbol{\nabla}\left(g_e - \frac{\delta T_{ze}}{T_{0e}}F_{0e}\right) = C[g_e] + \left(1 - \frac{v_z^2}{v_{\mathrm{th}e}^2}\right)F_{0e}\hat{\boldsymbol{b}}\cdot\boldsymbol{\nabla}\frac{e}{cm_e}d_e^2\nabla_\perp^2 A_z. \qquad [4]$$

In these equations, $d/dt \equiv \partial/\partial t + c/B_0\{\varphi, \ldots\}$ denotes the convective time derivative, with the Poisson bracket defined as $\{P, Q\} \equiv \partial_x P\partial_y Q - \partial_y P\partial_x Q$. The parallel (to the total field) gradient operator is $\hat{\boldsymbol{b}}\cdot\boldsymbol{\nabla}P \equiv \partial_z P - \{A_z, P\}/B_0$. The last term in the generalized Ohm's law features the (normalized) parallel electron temperature perturbation, defined in terms of the reduced electron distribution function as

$$\frac{\delta T_{ze}}{T_{0e}} = \frac{1}{n_{0e}}\left(\int d^3\boldsymbol{v}\frac{2v_z^2}{v_{\mathrm{th}e}^2}g_e\right); \qquad [5]$$

the isothermal limit of these equations corresponds to $\delta T_{ze} = 0$, that is, $g_e = 0$. Last, $C[g_e]$ represents the collision operator. Since Eq. **4** has no explicit dependence on $v_\perp$, this coordinate can be integrated out of the problem if a collision operator is chosen that bears no such dependence, such as the (modified) Lenard–Bernstein collision operator (34). In that case, the reduced distribution function becomes four-dimensional, $g_e = g_e(\boldsymbol{r}, v_z, t)$.

In the absence of collisions, Eqs. **2**–**4** conserve a quadratic invariant that is usually referred to as the total free energy

$$W \equiv \int\frac{d^3\boldsymbol{r}}{V}\left[\frac{1}{\tau}(1-\hat{\Gamma}_0)\frac{e^2 n_{0e}\varphi^2}{2T_{0e}} + \frac{|\nabla_\perp A_z|^2}{8\pi} + \frac{1}{\tau^2}(1-\hat{\Gamma}_0)^2\frac{e^2 n_{0e}\varphi^2}{2T_{0e}} + \frac{d_e^2|\nabla_\perp^2 A_z|^2}{8\pi} + \int d^3\boldsymbol{v}\frac{T_{0e}g_e^2}{2F_{0e}}\right], \qquad [6]$$

where the different terms on the right-hand side, in the order in which they appear, correspond to the ion perturbed entropy, the magnetic energy, the electron density variance, the kinetic energy of the parallel electron flow, and the electron free energy, respectively. For completeness, we note that the isothermal ($g_e = 0$) limit of these equations admits another ideal invariant—the generalized helicity,

$$H \equiv \int\frac{(1-\hat{\Gamma}_0)\varphi}{\rho_i^2}(1 - d_e^2\nabla_\perp^2)A_z dV, \qquad [7]$$

which reduces to $H \propto \int \delta n_e A_z dV$ in the range $\rho_i \gg k_\perp^{-1} \gg d_e$, and to the cross-helicity at MHD scales ($k_\perp\rho_i \ll 1$).

To better describe the velocity-space dynamics, we follow ref. 34 and expand $g_e$ in Hermite polynomials:

$$g_e(\boldsymbol{r}, v_z, t) = \frac{1}{\sqrt{2^m m!}}\sum_{m=0}^{\infty} H_m\left(\frac{v_z}{v_{\mathrm{th}e}}\right)g_m(\boldsymbol{r}, t)F_{0e}(v_z), \qquad [8]$$

where

$$g_m = \frac{1}{n_{0e}}\frac{1}{\sqrt{2^m m!}}\int_\infty^\infty dv_z H_m\left(\frac{v_z}{v_{\mathrm{th}e}}\right)g_e. \qquad [9]$$

Since $g_e$ only contains moments higher than $\delta n_e$ and $u_{ze}$, it follows that $g_0 = g_1 = 0$. Using the Hermite expansion, Eq. **4** can be

decomposed into a series of coupled equations for the Hermite coefficients $g_m$ (for $m \geq 2$):

$$\frac{dg_m}{dt} = -v_{\mathrm{th}e}\hat{\boldsymbol{b}}\cdot\boldsymbol{\nabla}\left(\sqrt{\frac{m+1}{2}}g_{m+1}+\sqrt{\frac{m}{2}}g_{m-1}-\delta_{m,1}g_2\right) - \sqrt{2}\delta_{m,2}\hat{\boldsymbol{b}}\cdot\boldsymbol{\nabla}\frac{e}{cm_e}d_e^2\nabla_\perp^2 A_z - C[g_m]. \quad [10]$$

At large $m$, free energy is converted to electron entropy and thence to heat via the collision operator $C[g_m]$.

In summary, the KREHM framework captures ion FLR effects and electron (drift) kinetic dynamics, including linear Landau damping. It is accurate at all scales above the electron Larmor radius, under the low-beta constraint $\beta_e \sim m_e/m_i$. The only linear mode captured by these equations is the kinetic Alfvén wave (KAW); as such, it provides the simplest-possible fully kinetic platform to study turbulence below the ion scales. In the long-wavelength limit $k_\perp\rho_i \ll 1$, the KREHM equations reduce to the reduced magnetohydrodynamic (RMHD) equations (35–38).

## Theoretical Models of Kinetic-Alfvén-Wave Turbulence

**Electromagnetic Fluctuations.** We first study the spectral properties of the electromagnetic fluctuations in the limit of isothermal electrons (i.e., $g_e$=0). In the framework that we adopt here (i.e., that provided by the KREHM equations), turbulent fluctuations at sub-$\rho_i$ scales are composed of nonlinearly interacting, strongly anisotropic KAWs. While we are formally restricted by the KREHM model to low $\beta$, we note that the KAW nature of sub-$\rho_i$ turbulence in more general contexts is widely supported [though not universally; see (e.g., refs. 39 and 40)] by numerical work (e.g., refs. 41–45) and observations (e.g., refs. 46–48). The total magnetic field is $\boldsymbol{B} = B_0\hat{\boldsymbol{z}} + \delta\boldsymbol{B}_\perp$, where the perpendicular (fluctuating) magnetic field is $\delta\boldsymbol{B}_\perp = -\hat{\boldsymbol{z}}\times\boldsymbol{\nabla}A_z$ and $\delta B_\perp/B_0 \ll 1$. The wave numbers of the fluctuations can be decomposed into parallel and perpendicular components (with respect to $\boldsymbol{B}$), $k_\parallel$ and $k_\perp$, corresponding to the correlation length of the fluctuations in the parallel direction and the perpendicular plane, $\ell \sim 1/k_\parallel$ and $\lambda \sim 1/k_\perp$, respectively. In the rest of the paper, we use the subscript $\lambda$ to refer to the amplitude of fluctuating quantities at scale $\lambda \sim k_\perp^{-1}$.

At $k_\perp\rho_i \gg 1$, the GK Poisson's law (Eq. **1**) reduces to

$$\delta n_{e\lambda}/n_{0e} \sim -e\varphi_\lambda/(\tau T_{0e}). \quad [11]$$

The scale-by-scale equipartition between the density and magnetic energy fluctuations (i.e., between the third and second terms in Eq. **6**), $(\delta n_e/n_{0e})^2 n_{0e}T_{0e} \sim |\nabla_\perp A_z|^2/8\pi$, combined with Eq. **11**, leads to the relation

$$\varphi_\lambda \sim (\rho_i V_A/c)\delta B_{\perp\lambda}, \quad [12]$$

with $V_A = B_0/\sqrt{4\pi\rho_0}$ the Alfvén speed pertaining to the guide field, where $\rho_0 = n_0 m_i$ is the background mass density.

Dynamically, the parallel component of fluctuations at scale $\ell \sim k_\parallel^{-1}$ is assumed to be determined by the propagation of KAWs, and so the characteristic (parallel) time scale is set by the (linear) frequency of those waves:

$$\gamma_l \sim \omega_{\mathrm{KAW}} \propto k_\perp\rho_s k_\parallel V_A \sim \rho_s V_A/(\ell\lambda), \quad [13]$$

where $\rho_s = \rho_i/\sqrt{2\tau}$ is the ion sound Larmor radius. The perpendicular fluctuations at scale $\lambda \sim k_\perp^{-1}$ undergo nonlinear interactions which lead to a cascade of constant energy flux toward smaller scales. Dimensionally, this inverse nonlinear time scale, usually referred to as the "eddy turnover rate," is

$$\gamma_{nl} \sim \varepsilon/(\rho_0 v_{A\lambda}^2/2) \sim \varepsilon/(\delta B_{\perp\lambda}^2/8\pi), \quad [14]$$

where $\varepsilon$ is the constant energy flux and $v_{A\lambda} = \delta B_{\perp\lambda}/\sqrt{4\pi\rho_0}$. The critical balance (2) conjecture declares that these two frequencies should be comparable at each scale, $\gamma_l \sim \gamma_{nl}$, setting the energy cascade rate of the turbulence. We denote by $E_B(k_\perp)$ the spectrum of magnetic energy and by $E_\varphi(k_\perp)$ the spectrum of the ion perturbed entropy $K_i$ (the first term on the *r.h.s.* of the total free energy invariant Eq. **6**). For $k_\perp\rho_i \gg 1$, $K_i$ reduces to the energy of density fluctuations, and for $k_\perp\rho_i \ll 1$ (in RMHD), $K_i$ reduces to the kinetic energy of the $\boldsymbol{E}\times\boldsymbol{B}$ flow. For scales above $d_e$, $K_i$ is expected to be in equipartition with the magnetic energy, while for scales below $d_e$, $K_i$ is expected to balance the kinetic energy of the parallel electron flows (the fourth term on the *r.h.s.* of Eq. **6**).

Different models for the nonlinear physics of the fluctuations lead to different predictions for the energy spectrum. A conventional Kolmogorov-like energy cascade yields a $\propto k_\perp^{-7/3}$ energy spectrum for magnetic and density fluctuations (22, 38, 49). This is significantly shallower than the approximate $-2.8$ power-law index (e.g., refs. 8, 50, and 51) that is widely found in solar-wind observations (7, 46–48, 52) and numerical simulations (28, 42, 53–57), implying that physics beyond standard Kolmogorov-like phenomenology is required to reconcile theory with observations. Noteworthy attempts in this direction include intermittency corrections (58) and tearing mediation (59), which both lead to the prediction of a $k_\perp^{-8/3}$ spectrum, despite the fact that the underlying physics is entirely different. In Zhou et al. (60), a detailed numerical study is performed and reaches the conclusion that in the isothermal limit (i.e., $g_e = 0$) of the KREHM framework, the magnetic and density fluctuations exhibit a $k_\perp^{-8/3}$ spectrum and that it is intermittency effects (58) that are responsible for the spectral steepening.

Rich as the physics is that underlies the above discussion, it is completely oblivious to electron kinetic effects (i.e., velocity-space dynamics triggered by allowing $g_e \neq 0$ in the KREHM equations), which introduce qualitatively different—and potentially just as important—physical phenomena. That is exactly the focus of our work, where we investigate the modifications to sub-$\rho_i$ turbulence due to electron kinetic physics. As we will show, velocity-space dynamics is as relevant to the understanding of KAW turbulence as real-space dynamics—and, indeed, we will demonstrate that the two are tightly connected.

**Phase-Space Cascade and Electron Heating.** The kinetic physics of electrons leads to complex dynamics in velocity space, relevant to energy dissipation and electron heating. In velocity space, the phase-mixing rate can be estimated through terms on the *r.h.s.* of Eq. **10** which represent the transfer of free energy from the $m$-th to $(m+1)$-th moment. In the large-$m$ limit, these terms can be written approximately as the derivative with respect to $m$, from which follows that the phase-mixing rate can be approximated as $\sim |k_\parallel|v_{\mathrm{th}e}/\sqrt{m} \sim (v_{\mathrm{th}e}/B_0)\{A_z,\ldots\}/\sqrt{m}$ (26, 34). In position space, on the other hand, free energy cascades to smaller spatial scales at the nonlinear-advection rate $d/dt \sim (c/B_0)\{\varphi,\ldots\}$ (*l.h.s.* of Eq. **10**). These rates are not, in general, the same. At each scale $\lambda$, there is a critical Hermite

mode number, denoted as $m_{\rm cr}$, at which these two rates balance:

$$\frac{c}{B_0}\{\varphi, g_{m_{\rm cr}}\} \sim \frac{v_{\rm the}}{B_0}\{A_z, g_{m_{\rm cr}}\}/\sqrt{m_{\rm cr}}, \qquad [15]$$

resulting in the relation $\sqrt{m_{\rm cr}} \sim (v_{{\rm th}e}/c)A_{z\lambda}/\varphi_\lambda$. At scales $k_\perp \rho_i \gg 1$, combined with the GK Poisson's law (Eq. **11**) and the equipartition relation (Eq. **12**), we obtain the spatial scale dependence of the critical Hermite order*:

$$m_{\rm cr}(\lambda) \sim (\lambda/d_e)^2/(2\tau). \qquad [16]$$

That is, for $\sqrt{m}k_\perp d_e \gg 1$, the nonlinear advection is expected to dominate, and the rapid coupling between modes with different $k_\parallel$ can result in a new mode with negative $k_\parallel$ and with a returning free-energy flux to lower Hermite moments. This classic phenomenon is known as the "plasma echo" (26, 30, 31).

In many astrophysical environments, collisions are so infrequent that the collisional cutoff in velocity space will only occur at asymptotically large $m$ ($\gg m_{\rm cr}$). Therefore, one may expect the free energy to reach $m_{\rm cr}$ and return to the low Hermite moments due to the restoring stochastic plasma echo. Kinetic turbulence would thus share the same dissipation route (real-space cascade) as fluid turbulence. However, this argument is seemingly at odds with measurements of strong electron heating in the near-Earth solar wind (11) and in kinetic simulations (61–63). Consistently, in the numerical results reported later in this paper, we observe no evidence for plasma echoes. We argue that this paradox is resolved by the presence of spontaneously formed current sheets in kinetic turbulent systems. On the one hand, efficient phase mixing is expected (as a result of the local suppression of nonlinearity) around current sheets (64, 65). On the other hand, it is at the sites with large gradient of current density (around the edge of current sheets) that most of the energy in fluid quantities is pumped into Hermite moments because the coupling between them is through $\propto \hat{\boldsymbol{b}}\cdot\boldsymbol{\nabla}(e/cm_e)d_e^2\nabla_\perp^2 A_z \propto \hat{\boldsymbol{b}}\cdot\boldsymbol{\nabla}J_z$ (last term in Eqs. **4** and **10**). The combination of these two effects of current sheets locally regulates the kinetic turbulence so that the free energy can freely transfer to large Hermite moments, unimpeded by echo, and collisionally dissipate, leading to electron heating. Therefore, the phase-mixing-dominated regime in phase space can be much wider than the estimation (Eq. **16**) based on the simple time-scale comparison (Eq. **15**).

**A Lowest-Order Solution for the Hermite-Expansion Coefficients of $g_e$.** Based on the time-scale comparison discussed in the previous section, we present a lowest-order solution for the perturbed electron distribution function $g_e$ in velocity space, valid in the absence of plasma echo. In Eq. **10**, each term can be ordered based on its inherent frequency. In the phase-mixing-dominated regime, the *l.h.s.* (proportional to the nonlinear-advection rate) of Eq. **10** is much smaller than its *r.h.s.* (proportional to the phase-mixing rate). To lowest order, the two terms on the *r.h.s.* should therefore balance, and each Hermite moment should satisfy the relation†

$$\begin{aligned} &g_{m+1} = -\sqrt{m/(m+1)}\,g_{m-1} \qquad \text{for } m \geq 3, \text{ and} \\ &g_3 = -2/\sqrt{3}\; e/(cm_e v_{\rm the})d_e^2\nabla_\perp^2 A_z. \end{aligned} \qquad [17]$$

That is, to the lowest order, all the odd Hermite moments share the same spatial configuration as the current, and all the even ones that of the temperature fluctuations, $g_2$.

The Hermite spectrum of $g_e$, $E_m \equiv \langle |g_m|^2\rangle/2$, where $\langle\ldots\rangle$ represents the volume average, can be derived from Eq. **17**. With the approximation $E_m \approx \langle |g_m||g_{m-1}|\rangle/2$ at large $m$, and using the relation $|g_{m+1}/g_{m-1}| = \sqrt{m/(m+1)}$, we obtain $E_{m+1}/E_{m-1} \approx g_{m+1}g_m/(g_{m-1}g_{m-2}) = \sqrt{(m-1)/(m+1)}$. This recursive relation leads to the solution $E_m \propto m^{-1/2}$—the same as the expected spectrum in a linear system with a Landau-damped kinetic field, corresponding to a constant flux of free energy transferring from small to large velocity moments (34, 66).

**Turbulence at Scales below the Electron Skin Depth, $\lambda \ll d_e$.** Last, one may also use the KREHM formalism to investigate the turbulent cascade at scales below $d_e$, i.e., in the range $\lambda \ll d_e \lesssim \rho_i$, where fluctuations become predominantly electrostatic. In this range, equipartition between the density fluctuations and kinetic energy of the parallel electron flows (i.e., between the third and fourth terms in Eq. **6**), $(\delta n_e/n_{0e})^2 n_{0e}T_{0e} \sim d_e^2|\nabla_\perp^2 A_z|^2/8\pi$, is expected, leading to the relation $\varphi_\lambda \sim (\rho_i V_A/c)d_e\delta B_{\perp\lambda}/\lambda$ (invoking Eq. **11**). As before, the critical Hermite moment, $m_{\rm cr}$, where the rate of free energy transfer between consecutive Hermite moments through linear phase mixing balances the nonlinear-advection rate, is estimated following Eq. **15**. Combined with the equipartition relation, we obtain $m_{\rm cr} \sim (\lambda/d_e)^4/(2\tau^2)$. That is, at scales $k_\perp d_e \gg 1$, the nonlinear advection of free energy is always faster than its channeling to larger Hermite moments. Linear phase mixing should therefore be subdominant as an energy dissipation channel, and the isothermal closure should be a good approximation to the dynamics at these scales.

Since neither the electron kinetic effects nor the electromagnetic effects [e.g., tearing mediation (59) or intermittency corrections (58)] are significant in this scale range, one might thus expect a standard Kolmogorov-type cascade model to be a reasonable description of turbulence at these scales. The energy flux of the cascade is $\varepsilon \sim \gamma_{\rm nl}e^2 n_{0e}\varphi^2/T_{0e}$, where the eddy turnover rate is $\gamma_{\rm nl} \sim \varphi_\lambda/\lambda^2$. Together with the equipartition relation, we obtain the kinetic and magnetic spectra

$$E_\varphi(k_\perp) \propto k_\perp^{-7/3}, \quad E_B(k_\perp) \propto k_\perp^{-13/3}. \qquad [18]$$

Imposing critical balance of these fluctuations, that is, $\omega_{\rm KAW} \sim \gamma_{nl}$ (at $k_\perp d_e \gg 1$, $\omega_{\rm KAW} \sim k_\parallel V_A \rho_s/d_e$), we obtain $k_\parallel \propto k_\perp^{4/3}$.

## Numerical Setup

We perform direct numerical simulations of the KREHM equations using the pseudospectral code Viriato (67). In what follows, quantities are given in dimensionless form. The domain is a triply periodic cubic box with sides of length $L = 2\pi$. Hyperdiffusion terms of the form $\nu_H\boldsymbol{\nabla}_\perp^6$ are included in the *r.h.s.* of Eq. **2** (electron hyperviscosity), Eq. **3** (hyperresistivity), and Eq. **10**, with $\nu_H$ dynamically adjusted to absorb energy at the grid scale (67). A hypercollision operator of the form $-\nu_{\rm coll}m^6$ is added to the *r.h.s.* of Eq. **10** for $m > 2$, with $\nu_{\rm coll}$ likewise set to remove energy at the smallest velocity scale, determined by $M$, the order of the highest Hermite polynomial kept in simulations. The simulations are driven with a white-noise forcing term added to Eq. **2**, which injects energy into the largest scales in the simulation box (perpendicular and parallel

*In critically balanced turbulence, the same result for $m_{\rm cr}$ is obtained if estimating $d/dt$ as $\omega_{\rm KAW}$ and balancing the two rates as $\omega_{\rm KAW} \sim k_\parallel v_{\rm the}/\sqrt{m_{\rm cr}}$.

†Strictly speaking, this argument only implies that the parallel gradients of the two Hermite moments on the *r.h.s.* of Eq. **10** should balance. Eq. **17** is a more stringent solution, and the fact that it is confirmed by our numerical results (see Fig. 4) is a nontrivial observation.

**Table 1. Summary of the key parameters of the simulations. $k_{\perp \max}$ is the maximum value of the perpendicular wavenumber, representing the spatial resolution in the perpendicular plane.**

| Runs | $\rho_i/L$ | $\rho_i/d_e$ | $k_{\perp\max}d_e$ | $M$ | $N^3$ |
|---|---|---|---|---|---|
| K1 | 0.1 | 20 | 0.9 | 30 | $256^3$ |
| K2a | 2 | 40 | 9 | 30 | $256^3$ |
| K2b | 2 | 20 | 9 | 60 | $128^3$ |
| K2c | 2 | 66 | 5.4 | 30 | $256^3$ |
| Iso | 2 | 66 | 5.4 | 0 | $256^3$ |
| K3 | 2 | 1 | 180 | 30 | $128^3$ |
| K4a-e | 3, 2, 1, 0.3, 0.1 | 30, 20, 10, 3, 1 | 9 | 30 | $128^3$ |

wavenumbers ranging from 1 to 2). Once a steady state is reached, the energy injection is balanced by its dissipation either through hypercollisions at large $m$ or through hyperdiffusion at large $k_\perp$, self-consistently determined by the nature of kinetic turbulence. As mentioned in the *Introduction*, it is one of the goals of this study to identify which of these dissipation channels is privileged by the turbulence.

The key simulation parameters are summarized in Table 1. We investigate three dynamical ranges of interest: 1) the inertial range $L > k_\perp^{-1} > \rho_i$, 2) the subion range $\rho_i > k_\perp^{-1} > d_e$, and 3) the electrostatic range $d_e > k_\perp^{-1}$. In run K1, we include both the inertial and sub-$\rho_i$ ranges, enabling us to study the transition across the $\rho_i$ scale. However, the resolution of the $d_e$ scale is sacrificed, and the effect of electron inertia on turbulence is not properly taken into account. This is compensated by runs K2(a,b) where the whole domain is in the subion range and $d_e$ is well resolved. Run K3 is designed to focus on the sub-$d_e$ range only. Runs K4(a-e) consist of a scan of the parameter $\rho_i/d_e$ with fixed $d_e$ and varying $\rho_i$ and are used to study the dependence of the energy dissipation on the scale separation between ion and electron scales.

## Numerical Results

In Fig. 1, we present results from the three main runs (K1, K2a, and K3, corresponding to the *Left*, *Middle*, and *Right* panels, respectively) that together cover the spatial scales ranging from MHD to sub-$d_e$. Run K1 captures the transition at $\rho_i$, and run K2 captures that at $d_e$. For each run, the results are plotted at an arbitrarily chosen time during the saturated stage of the turbulence.

**Visuals.** The top row shows the current densities normalized to their rms values on arbitrarily chosen $xy$ planes. The visualization of run K1 (*Left* panel) is dominated by the features of long-wavelength MHD turbulence, with indications of plasmoid instability (68) in some of the large-scale current sheets. At scales below $\rho_i$ (*Middle* panel), the current still exhibits sheet-type structures, but there are no visual signs of plasmoid generation. At scales below $d_e$ (*Right* panel), the current profile becomes less sharp and fewer finer structures appear in the system, consistent with the predicted steep magnetic spectrum (Eq. **18**) and with the fact that turbulence at these scales should be predominantly electrostatic.

**Energy Spectra.** The middle row shows the normalized perpendicular energy spectra of the magnetic and ion-entropy fluctuations, $\hat{E}_B(k_\perp)$ and $\hat{E}_\varphi(k_\perp)$. The main purpose of run K1 (*Left* panel) is to study the transition at around $k_\perp\rho_i \sim 1$, and so both the MHD range $k_\perp\rho_i < 1$ and the kinetic range $k_\perp\rho_i > 1$ are included in the simulation, with the compromise that neither of these two ranges is sufficiently wide to form a clear inertial range. In spite of this limitation, there is a clear steepening of the spectra at $k_\perp\rho_i \sim 1$. We observe $\hat{E}_B(k_\perp) \approx \hat{E}_\varphi(k_\perp)$ in the sub-$\rho_i$ range, confirming the assumption of equipartition between magnetic and density fluctuations (Eq. **12**).

The sub-$\rho_i$ range is explored in run K2a (*Middle* panel) where the transition at $k_\perp d_e \sim 1$ is well resolved. Both $\hat{E}_B(k_\perp)$ and $\hat{E}_\varphi(k_\perp)$ closely follow a $k_\perp^{-3}$ scaling until they deviate at scales below $d_e$. This is a steeper spectrum than the $k_\perp^{-8/3}$ spectrum in the isothermal limit, which is predicted (58) and numerically confirmed under the KREHM framework (58, 60). We attribute this steepening of the spectra to electron Landau damping, which enables the dissipation of a nonnegligible energy fraction via its cascade to high-order Hermite moments through phase mixing. This argument will be elaborated and tested below (around Fig. 2). At scales below $d_e$ (run K3, *Right* panel), $\hat{E}_B(k_\perp) \propto k_\perp^{-13/3}$ and $\hat{E}_\varphi(k_\perp) \propto k_\perp^{-7/3}$ are measured, confirming the predictions for the electrostatic limit (Eq. **18**).

**Energy Dissipation.** The *Bottom* row of Fig. 1 shows contour maps of the normalized (to its maximum value) dissipation rate of the total free energy (defined in Eq. **6**) in the $m$-$k_\perp$ phase space. Here, the $m = 0$ and $m = 1$ moments correspond to $\delta n_e/n_{0e}$ and $A_z$, respectively (and we remind the reader that all fields can be damped in real space by hyperdiffusion and that Hermite moments $m > 2$ can also access velocity-space dissipation via hypercollisions, as described in *Numerical Setup*). These results directly address one of the main questions in this paper—the competition between the kinetic and fluid channels for energy dissipation. In run K1 (*Left* panel), we focus on the MHD range and the transition to sub-$\rho_i$ scales. The strong energy dissipation at large ($m \gg 1$) Hermite moments turns on at around the $\rho_i$ scale and extends toward smaller scales (larger $k_\perp$), suggesting the domination of phase mixing over nonlinear advection at those scales.[‡] Because $d_e$ is unresolved in this run, the energy flux in position space reaches the (hyper)viscous scale without going through the full kinetic range. This truncation of electron kinetic effects at large $k_\perp$ causes an artificially strong dissipation by the hyperviscosity (and resistivity), preventing us from making a direct comparison of dissipation at large $m$ and large $k_\perp$ in this run. This issue is resolved in run K2a (*Middle* panel). With the understanding that the large-$m$ dissipation turns on at $k_\perp\rho_i \sim 1$, we can study the sub-$\rho_i$ range scale and focus on the range between $\rho_i$ and $d_e$, with $d_e$ properly resolved. With electron kinetic physics fully accounted for, we find that most of the energy is dissipated at large $m$ and at around $\rho_i$ scales. This result is direct evidence of the absence of plasma echo in the range between $\rho_i$ and $d_e$ and clearly demonstrates that the kinetic channel is dominant for energy dissipation: the free energy transfers to small scales in velocity space through phase mixing, where it dissipates via collisions and heats the electrons. The strong electron heating at $k_\perp\rho_i \gtrsim 1$ is consistent with earlier gyrokinetic studies (23, 55). Although the damping rate of KAWs is relatively small at $k_\perp\rho_i \approx 1$ (*SI Appendix*, Fig. S1), the steep ($\sim k_\perp^{-3}$) energy spectra ensure a much larger amount of electromagnetic energy subject to Landau damping at around $\rho_i$ than that at around $d_e$.

[‡]The large-$m$ dissipation at the system scale is artificial, caused by the forcing.

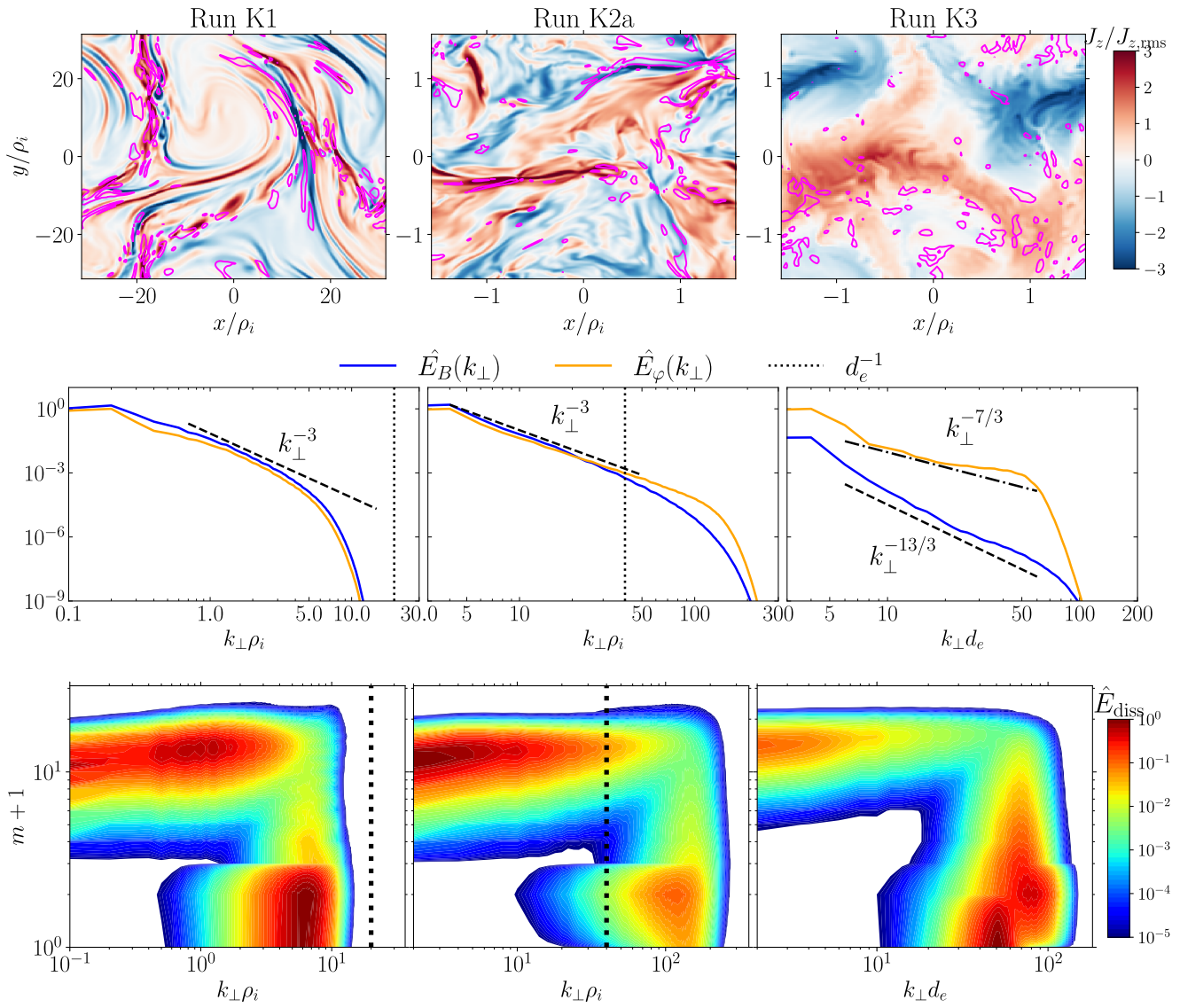


**Fig. 1.** Runs K1 (*Left column*), K2a (*Middle column*), and K3 (*Right column*). *Top*: visualization of $J_z$ (color map). The magenta lines are the contours of the electron heating rate that is twice its volume-averaged value. *Middle*: Magnetic energy and density spectra. *Bottom*: Energy dissipation spectra in $m$-$k_\perp\rho_i$ phase space. The vertical dotted lines indicate the $d_e$ scale.

The large-$m$ dissipation starting at the lowest $k_\perp$ turns off at around the $d_e$ scale. To explore the sub-$d_e$ range, we analyze run K3 (*Right* panel), and find that the energy dissipation at large $k_\perp$ is clearly dominant. This is consistent with our prediction that although the Landau damping rate of linear KAWs is large in the sub-$d_e$ range, the nonlinear advection is faster than the phase-mixing process, causing the energy flux to mainly cascade to, and dissipate at, large $k_\perp$ rather than large $m$.

**Landau Damping of KAWs.** In order to confirm that the strong energy dissipation at high $m$ is indeed caused by the Landau damping of KAWs, we test the following argument with our numerical results. Let us assume that at each scale $k_\perp^{-1}$, the electromagnetic fluctuations are damped at the KAW linear damping rate pertaining to that scale, $\gamma_{\mathrm{KAW}}(k_\perp)$. Then, within a nonlinear cascade time $1/\gamma_{nl}$—which, by assumption of critical balance, is comparable to the linear time scale, $1/\gamma_{nl} \sim 1/\omega_{\mathrm{KAW}}$—a fraction of $\sim 2\gamma_{\mathrm{KAW}}/\omega_{\mathrm{KAW}}$ of the magnetic energy is damped and becomes the free energy in $g_e$. All the mentioned quantities are scale-dependent. With this assumption, if we consider a magnetic spectrum from a simulation with isothermal electrons, $\hat{E}_B^{\mathrm{iso}}(k_\perp)$, and subtract from it the energy that would be Landau-damped within a cascade time, it should match the spectrum $\hat{E}_B^{\mathrm{K}}$ from the corresponding kinetic simulation (i.e., a simulation that differs from the isothermal one only in allowing for kinetic electrons, $g_e \neq 0$):

$$\hat{E}_B^{\mathrm{K}}(k_\perp) \approx \hat{E}_B^{\mathrm{iso}}(k_\perp)(1 - 2\gamma_{\mathrm{KAW}}/\omega_{\mathrm{KAW}}). \qquad [19]$$

This conjecture is confirmed in the comparison of spectra from run K2a and its corresponding isothermal run (Iso), shown in Fig. 2, where the scale-dependent $\gamma_{\mathrm{KAW}}$ and $\omega_{\mathrm{KAW}}$ are calculated from the linear dispersion relation of KAWs (see *SI Appendix* for more details). This agreement suggests that the magnetic spectra from kinetic runs, shown in this figure and in Fig. 1, which we tentatively fitted with a $k_\perp^{-3}$ scaling, are, in fact, not a simple power law, but rather a more complicated function well approximated by [**19**]. Incidentally, we note that it should not be

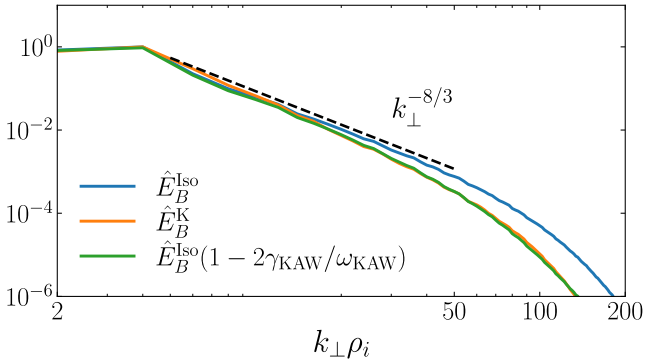


**Fig. 2.** Comparison between the magnetic spectrum from run K2c ($\hat{E}_B^{\rm K}$) and that from run Iso ($\hat{E}_B^{\rm Iso}$) multiplied by a scale-dependent factor ($1 - 2\gamma_{\rm KAW}/\omega_{\rm KAW}$) that represents the subtraction of the Landau-damped energy within a cascade time.

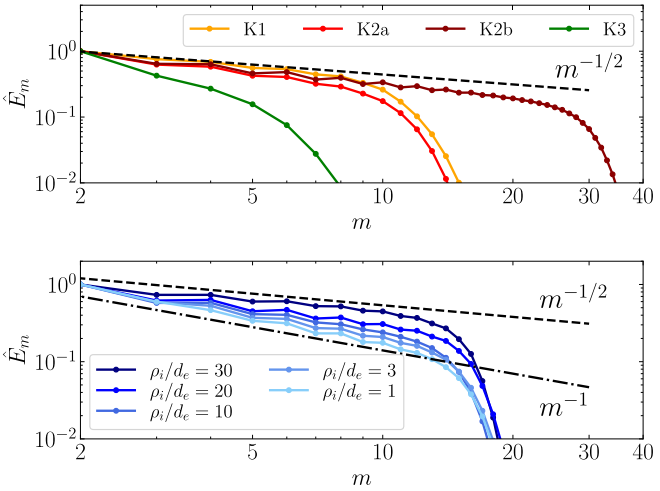


**Fig. 3.** Normalized Hermite spectra from simulations K1-K3 (*Top*) and K4a-e (*Bottom*).

an artifact of numerical simulations that the sub-$\rho_i$ spectra do not exhibit power-law scalings, since the scale separation between $\rho_i$ and $d_e$ in our simulation is not far-off from that in realistic systems such as the solar wind. This result is consistent with the weakened cascade model originally proposed by Howes et al. (69, 70) and numerically tested by TenBarge and coworkers (71, 72). In the next sections of this paper, we provide the physical explanation for Landau damping to be the dominant heating mechanism. In a broader context, the result presented in Fig. 2 provides a justification for a model (73–76) that is widely used in studies of turbulent astrophysical systems, which is based on the assumption that we just confirmed: that the effect of phase mixing is merely to damp the turbulent cascade of the electromagnetic fluctuations at a scale-dependent rate set by linear electron Landau damping.

**Hermite Moments of $g_e$.** Strong energy dissipation at high Hermite mode numbers $m \gg 1$ requires a significant energy cascade toward small scales in the velocity space and should thus correspond to a shallow Hermite spectrum. This is consistent with our numerical results shown in the top panel of Fig. 3. For runs K1 and K2a with strong large-$m$ dissipation, we measure a shallow $m^{-1/2}$ spectrum. In contrast, for run K3 where large-$m$ dissipation is weak and large-$k_\perp$ dissipation dominates, a much steeper Hermite spectrum is measured. The $m^{-1/2}$ spectrum in run K1 is consistent with our earlier explanation that although the dissipation at large-$k_\perp$ is significant in this case, it is due to the truncation of electron kinetic physics at the hyperviscous scale, and a significant phase-mixing-dominated energy cascade in velocity space does exist at spatial scales larger than the hyperviscous scale.

In the bottom panel of Fig. 3, we show the Hermite spectra from runs with different values of $\rho_i/d_e$. In these runs, $d_e$ is fixed at small scales (but resolved). A large value of $\rho_i/d_e$ corresponds to a wider electromagnetic sub-$\rho_i$ range where KAWs exist and are subject to Landau damping, whereas runs with small $\rho_i/d_e$ are mostly in the MHD range. As shown, decreasing values of $\rho_i/d_e$, i.e., a narrower dynamical range for Landau-damped KAWs, results in a progressively steeper Hermite spectrum. This result further confirms the significant contribution of the Landau damping of KAWs to velocity-space dissipation.

The $m^{-1/2}$ scaling is predicted by our analytical model based on the timescale ordering between the KAW frequency (which is also the cascade rate) and the phase mixing rate: $\omega_{\rm KAW} \ll k_\parallel v_{\rm the}/\sqrt{m}$; this leads to a lowest-order solution relating different Hermite moments, Eq. **17**. To further test our theory, we measure the correlation between Hermite moments $g_{m-1}$ and $g_{m+1}$, a few examples of which are shown in Fig. 4, *Top* and *Middle* panels. The measured correlations between $J_z$ and $g_3$, $g_5$ and $g_3$, $g_4$ and $g_2$, and between $g_6$ and $g_4$ exhibit remarkable agreement with our lowest-order solution $g_3 = 2/\sqrt{3}(d_e/\rho_s)J_z$ (in code units) and $g_{m+1} = -\sqrt{m/(m+1)}g_{m-1}$ for $m \geq 3$ (Eq. **17**).

**Absence of Plasma Echoes.** The unimpeded Hermite cascade of energy that we observe implies that the stochastic echo effect that we discussed earlier is negligible in our simulations. It is revealing to understand why that should be so. The time-scaling ordering leads to a critical Hermite mode number $m_{\rm cr} \sim (\lambda/d_e)^2/(2\tau^2)$ (Eq. **16**), below which the phase mixing is faster than the nonlinear advection, and above which the advection can in principle dominate the phase mixing to establish the plasma echo. That seems to indicate that for a system with asymptotically large cutoff $M$, the plasma echo should always occur, causing a returning energy flux to low Hermite moments and thus strong energy dissipation at large $k_\perp$. Even for a system with limited $M$

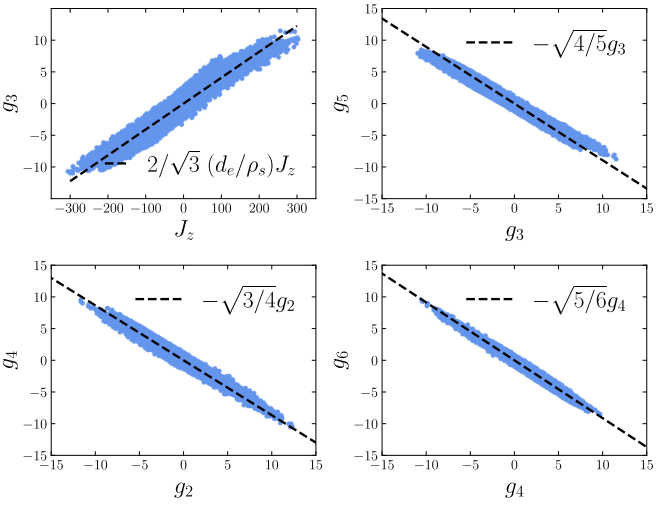


**Fig. 4.** Scatter plots from simulation K1 showing the correlation between $J_z$ and $g_3$ (*Top left*), $g_5$ and $g_3$ (*Top right*), $g_4$ and $g_2$ (*Bottom left*), and between $g_6$ and $g_4$ (*Bottom right*).

(as that in our simulations), at sufficiently small scale $\lambda$, $m_{cr}$ will be resolved ($m_{cr} < M$), and phase mixing should be suppressed at those scales. However, these arguments are contradictory to our numerical results of the $m^{-1/2}$ Hermite spectrum and efficient electron heating.

To further confirm the absence of echo, we perform two additional runs, K2b and K4b, between which the only difference is the number of Hermite moments ($M = 30$ for K4b and $M = 60$ for K2b). The Hermite spectrum of K2b also exhibits a $m^{-1/2}$ scaling (Fig. 3, *Top* panel). In Fig. 5, we compare the dissipation rate of total free energy between the K2b ($M = 60$) and K4b ($M = 30$) runs (dashed and solid blue curves). The good overlap indicates that the features of energy dissipation remain unchanged when including more Hermite moments and thus extending the range of spatial scales over which a potential plasma echo could arise. In the same figure, we follow Eq. **16** and plot the dependence of the critical Hermite mode number $m_{cr}$ on $k_\perp \rho_i$ (red curve). Based on the comparison between advection and phase-mixing rates (Eq. **15**), the plasma echo is allowed in the region above the red curve and below the cutoff $M$, which is a wide region for both runs. Therefore, the plasma echo is absent not because it is excluded in our simulations due to limited resolution in position or velocity space; instead, its absence must be due to the turbulent dynamics.

We proposed in the theory section that the absence of echo is due to the local reduction of the advective nonlinearity around current sheets. The visuals of $J_z$ (Fig. 1, *Top* panels) show that indeed, at scales larger than $d_e$, the regions with strong current density are elongated "sheet" structures. In Fig. 6, we show the ratio of the nonlinear-advection rate to the phase-mixing rate of $g_7$ versus the normalized current density (the results using other Hermite moments are qualitatively similar); the color map of the data points represents the local energy density of $g_7$. This plot clearly shows that nonlinear advection is subdominant with respect to phase mixing at positions with large current density. We conjecture that it is the specific configuration of $A_z$, $\varphi$, and $g_m$ around the sheet-like structure of current that leads to the local suppression of echo effects; this interpretation is inspired by observations of strong phase mixing in supposedly similar geometries that arise in reconnection studies (64, 65, 77) [Note that simply invoking the quasi-1D (in the perpendicular plane) morphology of current sheets is not sufficient to explain

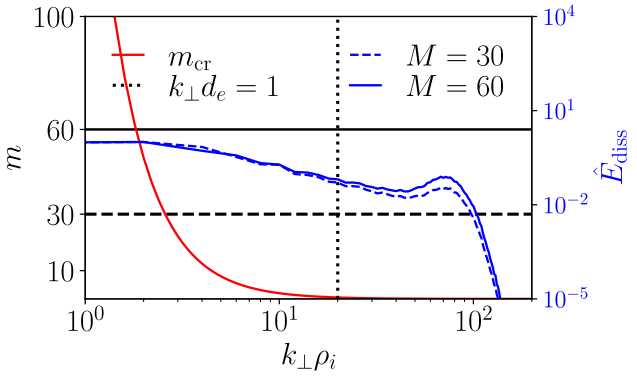


**Fig. 5.** Comparison between normalized total energy dissipation spectra (integrated over $m$) between run K2b (with $M = 60$; blue solid curve) and run K4b (with $M = 30$; blue dashed line). Also in the figure is the dependence of the critical Hermite moment order, $m_{cr}$ (Eq. **16**), as a function of $k_\perp \rho_i$. The horizontal lines indicate the cutoff of $m$ at 30 and 60. For both $M = 30$ and $M = 60$ runs, a wide range of wavenumbers exists that in principle allows plasma echo to occur.

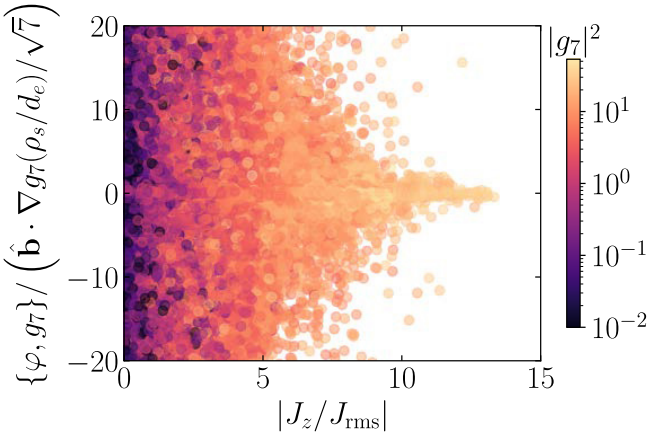


**Fig. 6.** The ratio of the nonlinear-advection rate to phase-mixing rate of $g_7$ as a function of normalized current density $|J_z/J_{rms}|$. The color corresponds to the local energy density of $g_7$.

the weakening of the advection-to-phase-mixing rates because such weakening would affect equally the advective nonlinearity and the parallel streaming]. As a result of enhanced phase mixing, current sheets are also where the $g_m$ fluctuations are concentrated (Eq. **17**), as shown by the correlation between $|g_7|^2$ and $|J_z/J_{rms}|$ in Fig. 6. Therefore, current sheets are energetically important for dissipation. The overlap in position space between the suppression of plasma echo and the concentration of free energy in $g_e$ results in the efficient energy transfer to small scales in velocity space and, eventually, strong electron heating at the kinetic range.

To further visualize this correlation between the current density and electron heating, in the color map of current density (Fig. 1, *Top* panels), we show the regions with strong electron heating using the contour (magenta lines) of the electron heating rate (measured by the energy dissipation through hypercollisions at small scales in velocity space) that is twice its volume-averaged value. Indeed, we find that for scales such that $\rho_i \simeq k_\perp^{-1} > d_e$ (*Left* and *Middle* panels), significant electron heating mostly occurs around current sheets, consistent with the above arguments. Such correlation between heating and current sheets has been reported in numerical simulations of kinetic turbulence (23, 72) and observations (78). Here, we add to the previous body of work by showing how such heating is possible: the reduction of the advective nonlinearity around current sheets enables phase-mixing to proceed unimpeded in those locations.

## Conclusions

In this work, we conduct an analytical and numerical study of subion-gyroscale (sub-$\rho_i$) turbulence in the low-$\beta$ limit using an analytical formalism known as the KREHM (34). We study the phase-space dynamics and channels for energy dissipation to understand the physical mechanism for electron heating. In the $m$-$k_\perp$ phase space, where $m$ is the velocity-space mode number, the energy dissipation is found to mostly occur at high $m$ through collisions, implying that phase mixing dominates nonlinear advection of the free energy and, thus, that the "kinetic channel" (as opposed to the "fluid channel") is the main route for energy dissipation and electron heating. We verify that this argument is quantitatively supported, as follows: if we subtract from the magnetic spectrum pertaining to an isothermal run the energy that would be linearly Landau-damped within one eddy

turnover time, scale by scale, we obtain a spectrum that agrees remarkably well with that from a corresponding run with kinetic electrons (see also refs. 69–72). A direct consequence of this result is that the application of a Landau-fluid-type closure (79) to KAW turbulence in the low-$\beta$ limit is justified.

We derive a lowest-order solution for the coefficients of the Hermite expansion of the electron distribution function, $g_m$, under the assumption that phase mixing dominates over nonlinear advection: $g_{m+1} = -\sqrt{m/(m+1)}g_{m-1}$, and $g_3 \propto J_z$. This solution, as well as the corresponding $m^{-1/2}$ Hermite spectrum, is confirmed by our numerical results. Last, we find that the absence of stochastic plasma echo, which would impede phase mixing, is due to the ubiquitous current sheets that develop self-consistently in our system. The fluctuations of the Hermite moments are concentrated in the vicinity of current sheets, while at these specific positions, the advective nonlinearity is weakened because of the specific configurations of the magnetic field and the flow around the sheets. This observed anticorrelation between advective nonlinearity and current density (and thus the density of free energy) undermines plasma echo and allows the free energy to transfer to higher $m$ by phase mixing.

There are several astrophysical environments of interest where $\beta$ is sufficiently small that the KREHM model should apply, such as ionospheric plasmas (80, 81), regions of solar wind and corona (82–84), and Earth's magnetosheath (85). However, further research is required to generalize the results obtained in the KREHM framework to a broader context. Based on existing numerical studies (24, 65), the KREHM model agrees well with full gyrokinetics at values of $\beta$ that are quite outside its region of asymptotic validity. Pertinently, in Grošelj et al. (24), it was found that KREHM agrees rather well not only with gyrokinetics, but also with a fully kinetic particle-in-cell approach in a simulation of decaying two-dimensional (86) turbulence at $\beta = 0.1$. These studies suggest that the results reported in this paper should be relevant to astrophysical environments beyond the low-$\beta$ limit—a speculation further supported by the many previous studies (performed at a range of values of $\beta$) that highlight the critical role of current sheets as dissipative structures in collisionless turbulence (e.g., refs. 54, 71, 72, 87). The efficient electron heating we found in the low-$\beta$ limit is qualitatively consistent with previous numerical studies on electron versus ion energization in kinetic turbulence, in which the electron to ion heating rate ratio is a decreasing function of plasma $\beta$ (e.g., refs. 74, 88–90). In a gyrokinetic study of reconnection (65), it is found that ion heating (via nonlinear phase mixing) becomes progressively more important as $\beta$ increases. Extrapolating these ideas to kinetic turbulence suggests that as $\beta$ increases (but still below unity), current sheets remain critical as energy dissipation sites, with the balance shifting from heating electrons at low beta (via linear phase mixing) to ions (via nonlinear phase mixing). Further studies are required to test this hypothesis.

In addition to critical plasma parameters such as the plasma $\beta$ and temperature ratio, the effects of the "large-scale" conditions of the turbulence on the energy dissipation are also to be investigated. For example, the imbalance of turbulence relevant to the fast-wind streams has recently been found to have profound effects on the heating mechanisms for ions and electrons (91, 92), while the electron kinetic effects are omitted. Kinetic studies taking into account both electron and ion physics with relevant large-scale conditions are necessary to explain the extensive measurements taken both at corona and the solar wind by currently operating and future spacecrafts.

**Data, Materials, and Software Availability.** HDF5 data have been deposited in Zenodo (https://doi.org/10.5281/zenodo.7789881). This data set contains the raw date from the main runs (run K1, run K2a, run K3) for the manuscript Electron heating in kinetic-Alfvén-wave turbulence. It contains the full data of density perturbation ($n_e$), magnetic potential ($A_z$), the perturbed distribution function of electrons ($g_e$), as well as the Fourier and Hermite spectra for the snapshots that are analyzed in the manuscript (93).

**ACKNOWLEDGMENTS.** We thank L. Arzamasskiy, S. Boldyrev, G. Howes, N. Mandell, R. Meyrand, A. A. Schekochihin, J. TenBarge, and V. Zhdankin for insightful discussions. This work was supported by the NSF under CAREER award No. 1654168 (N.F.L. and M.Z.), by the NASA under award NNH19ZA001N-FINESST (M.Z.), and by the NSF-DOE Partnership in Basic Plasma Science and Engineering Award No. PHY-2010136 (Z.L.). This research used resources of the MIT-PSFC partition of the Engaging cluster at the MGHPCC facility, funded by DOE award No. DE-FG02-91-ER54109 and the National Energy Research Scientific Computing Center, a DOE Office of Science User Facility supported by the Office of Science of the US Department of Energy under Contract No. DE-AC02-05CH11231 using NERSC award FES-ERCAP0020063.

1. J. E. Borovsky, H. O. Funsten, MHD turbulence in the Earth's plasma sheet: Dynamics, dissipation, and driving. *J. Geophys. Res.: Space Phys.* **108**, 1284 (2003).
2. P. Goldreich, S. Sridhar, Toward a theory of interstellar turbulence. II. Strong alfvenic turbulence. *Astrophys. J.* **438**, 763–775 (1995).
3. C. Y. Tu, E. Marsch, MHD structures, waves and turbulence in the solar wind: Observations and theories. *Space Sci. Rev.* **73**, 1–210 (1995).
4. E. N. Parker, Magnetic neutral sheets in evolving fields. I–General theory. *Astrophys. J.* **264**, 635–647 (1983).
5. S. A. Balbus, J. F. Hawley, Instability, turbulence, and enhanced transport in accretion disks. *Rev. Mod. Phys.* **70**, 1 (1998).
6. M. C. Begelman, A. C. Fabian, Turbulent mixing layers in the interstellar and intracluster medium. *Mon. Not. R. Astron. Soc.* **244**, 26P–29P (1990).
7. F. Sahraoui, M. L. Goldstein, P. Robert, Y. V. Khotyaintsev, Evidence of a cascade and dissipation of solar-wind turbulence at the electron gyroscale. *Phys. Rev. Lett.* **102**, 231102 (2009).
8. O. Alexandrova *et al.*, Universality of solar-wind turbulent spectrum from MHD to electron scales. *Phys. Rev. Lett.* **103**, 165003 (2009).
9. O. Alexandrova, C. Lacombe, A. Mangeney, R. Grappin, M. Maksimovic, Solar wind turbulent spectrum at plasma kinetic scales. *Astrophys. J.* **760**, 121 (2012).
10. O. Alexandrova, C. H. K. Chen, L. Sorriso-Valvo, T. S. Horbury, S. D. Bale, Solar wind turbulence and the role of ion instabilities. *Space Sci. Rev.* **178**, 101–139 (2013).
11. C. H. K. Chen, K. G. Klein, G. G. Howes, Evidence for electron Landau damping in space plasma turbulence. *Nat. Commun.* **10**, 1–8 (2019).
12. T. N. Parashar *et al.*, Turbulent dissipation challenge: A community-driven effort. *J. Plasma Phys.* **81**, 905810513 (2015).
13. P. Dmitruk, W. H. Matthaeus, N. Seenu, Test particle energization by current sheets and nonuniform fields in magnetohydrodynamic turbulence. *Astrophys. J.* **617**, 667 (2004).
14. W. H. Matthaeus , M. Velli , Who needs turbulence? A review of turbulence effects in the heliosphere and on the fundamental process of reconnection. *Space Sci. Rev.* **160**, 145–168 (2011).
15. S. Servidio *et al.*, Magnetic reconnection as an element of turbulence. *Nonlinear Process. Geophys.* **18**, 675–695 (2011).
16. K. T. Osman, W. H. Matthaeus, A. Greco, S. Servidio, Evidence for inhomogeneous heating in the solar wind. *Astrophys. J. Lett.* **727**, L11 (2011).
17. V. Zhdankin, D. A. Uzdensky, J. C. Perez, S. Boldyrev, Statistical analysis of current sheets in three-dimensional magnetohydrodynamic turbulence. *Astrophys. J.* **771**, 124 (2013).
18. S. Chapman, T. G. Cowling, *The Mathematical Theory of Non-uniform Gases: An Account of the Kinetic Theory of Viscosity, Thermal Conduction and Diffusion in Gases* (Cambridge University Press, 1990).
19. A. Hasegawa, L. Chen, Plasma heating by Alfvén-wave phase mixing. *Phys. Rev. Lett.* **32**, 454 (1974).
20. J. Heyvaerts, E. R. Priest, Coronal heating by phase-mixed shear Alfven waves. *Astron. Astrophys.* **117**, 220–234 (1983).
21. A. A. Schekochihin *et al.*, Gyrokinetic turbulence: A nonlinear route to dissipation through phase space. *Plasma Phys. Controll. Fus.* **50**, 124024 (2008).
22. G. G. Howes *et al.*, A model of turbulence in magnetized plasmas: Implications for the dissipation range in the solar wind. *J. Geophys. Res.: Space Phys.* **835**, 137 (2008).
23. A. B. Navarro *et al.*, Structure of plasma heating in gyrokinetic Alfvénic turbulence. *Phys. Rev. Lett.* **117**, 245101 (2016).
24. D. Grošelj *et al.*, Fully kinetic versus reduced-kinetic modeling of collisionless plasma turbulence. *Astrophys. J.* **847**, 28 (2017).
25. S. Servidio *et al.*, Magnetospheric multiscale observation of plasma velocity–space cascade: Hermite representation and theory. *Phys. Rev. Lett.* **119**, 205101 (2017).
26. A. A. Schekochihin *et al.*, Phase mixing versus nonlinear advection in drift-kinetic plasma turbulence. *J. Plasma Phys.* **82**, 905820212 (2016).
27. T. Adkins, A. A. Schekochihin, A solvable model of Vlasov-kinetic plasma turbulence in Fourier–Hermite phase space. *J. Plasma Phys.* **84**, 905840107 (2018).
28. S. S. Cerri, M. W. Kunz, F. Califano, Dual phase-space cascades in 3D hybrid-Vlasov–Maxwell turbulence. *Astrophys. J. Lett.* **856**, L13 (2018).

29. G. L. Eyink, Cascades and dissipative anomalies in nearly collisionless plasma turbulence. *Phys. Rev. X* **8**, 041020 (2018).
30. R. W. Gould, T. M. O'Neil, J. H. Malmberg, Plasma wave echo. *Phys. Rev. Lett.* **19**, 219–222 (1967).
31. J. H. Malmberg, C. B. Wharton, R. W. Gould, T. M. O'Neil, Plasma wave echo experiment. *Phys. Rev. Lett.* **20**, 95 (1968).
32. R. Meyrand, A. Kanekar, W. Dorland, A. A. Schekochihin, Fluidization of collisionless plasma turbulence. *Proc. Natl. Acad. Sci. U.S.A.* **116**, 1185–1194 (2019).
33. J. T. Parker, E. Highcock, A. A. Schekochihin, P. Dellar, Suppression of phase mixing in drift-kinetic plasma turbulence. *Phys. Plasmas* **23**, 070703 (2016).
34. A. Zocco, A. A. Schekochihin, Reduced fluid-kinetic equations for low-frequency dynamics, magnetic reconnection, and electron heating in low-beta plasmas. *Phys. Plasmas* **18**, 102309 (2011).
35. B. B. Kadomtsev, O. P. Pogutse, Nonlinear helical perturbations of a plasma in the tokamak. *Sov. Phys. J. Exp. Theor. Phys.* **5**, 575–590 (1973).
36. H. R. Strauss, Nonlinear, three-dimensional magnetohydrodynamics of noncircular tokamaks. *Phys. Fluids* **19**, 134–140 (1976).
37. G. P. Zank, W. H. Matthaeus, The equations of reduced magnetohydrodynamics. *J. Plasma Phys.* **48**, 85–100 (1992).
38. A. A. Schekochihin *et al*., Astrophysical gyrokinetics: Kinetic and fluid turbulent cascades in magnetized weakly collisional plasmas. *Astrophys. J. Suppl. Ser.* **182**, 310 (2009).
39. S. Galtier, A. Bhattacharjee, Anisotropic weak whistler wave turbulence in electron magnetohydrodynamics. *Phys. Plasmas* **10**, 3065–3076 (2003).
40. D. Shaikh, G. P. Zank, Spectral features of solar wind turbulent plasma. *Mon. Not. R. Astron. Soc.* **400**, 1881–1891 (2009).
41. S. P. Gary, K. Nishimura, Kinetic Alfvén waves: Linear theory and a particle-in-cell simulation. *J. Geophys. Res.: Space Phys.* **109**, A02109 (2004).
42. J. M. TenBarge, J. J. Podesta, K. G. Klein, G. G. Howes, Interpreting magnetic variance anisotropy measurements in the solar wind. *Astrophys. J.* **753**, 107 (2012).
43. L. Franci, S. Landi, A. Verdini, L. Matteini, P. Hellinger, Solar wind turbulent cascade from MHD to sub-ion scales: Large-size 3D hybrid particle-in-cell simulations. *Astrophys. J.* **853**, 26 (2018).
44. S. S. Cerri, D. Grošelj, L. Franci, Kinetic plasma turbulence: Recent insights and open questions from 3D3V simulations. *Front. Astron. Space Sci.* **6**, 64 (2019).
45. D. Grošelj *et al*., Kinetic turbulence in astrophysical plasmas: Waves and/or structures? *Phys. Rev. X* **9**, 031037 (2019).
46. R. J. Leamon, C. W. Smith, N. F. Ness, W. H. Matthaeus, H. K. Wong, Observational constraints on the dynamics of the interplanetary magnetic field dissipation range. *J. Geophys. Res.: Space Phys.* **103**, 4775–4787 (1998).
47. C. S. Salem *et al*., Identification of kinetic Alfvén wave turbulence in the solar wind. *Astrophys. J. Lett.* **745**, L9 (2012).
48. C. H. K. Chen, S. Boldyrev, Q. Xia, J. C. Perez, Nature of subproton scale turbulence in the solar wind. *Phys. Rev. Lett.* **110**, 225002 (2013).
49. J. Cho, A. Lazarian, The anisotropy of electron magnetohydrodynamic turbulence. *Astrophys. J. Lett.* **615**, L41 (2004).
50. K. H. Kiyani, S. C. Chapman, Y. V. Khotyaintsev, M. W. Dunlop, F. Sahraoui, Global scale-invariant dissipation in collisionless plasma turbulence. *Phys. Rev. Lett.* **103**, 075006 (2009).
51. F. Sahraoui *et al*., Scaling of the electron dissipation range of solar wind turbulence. *Astrophys. J.* **777**, 15 (2013).
52. S. D. Bale, P. J. Kellogg, F. S. Mozer, T. S. Horbury, H. Reme, Measurement of the electric fluctuation spectrum of magnetohydrodynamic turbulence. *Phys. Rev. Lett.* **94**, 215002 (2005).
53. S. Servidio *et al*., A kinetic model of plasma turbulence. *J. Plasma Phys.* **81**, 325810107 (2015).
54. M. Wan *et al*., Intermittent dissipation and heating in 3D kinetic plasma turbulence. *Phys. Rev. Lett.* **114**, 175002 (2015).
55. D. Told, F. Jenko, J. M. TenBarge, G. G. Howes, G. Hammett, Multiscale nature of the dissipation range in gyrokinetic simulations of Alfvénic turbulence. *Phys. Rev. Lett.* **115**, 025003 (2015).
56. L. Arzamasskiy, M. W. Kunz, B. D. G. Chandran, E. Quataert, Hybrid-kinetic simulations of ion heating in Alfvénic turbulence. *Astrophys. J.* **879**, 53 (2019).
57. D. Grošelj, A. Mallet, N. F. Loureiro, F. Jenko, Fully kinetic simulation of 3D kinetic Alfvén turbulence. *Phys. Rev. Lett.* **120**, 105101 (2018).
58. S. Boldyrev, J. C. Perez, Spectrum of kinetic-Alfvén turbulence. *Astrophys. J. Lett.* **758**, L44 (2012).
59. N. F. Loureiro, S. Boldyrev, Collisionless reconnection in magnetohydrodynamic and kinetic turbulence. *Astrophys. J.* **850**, 182 (2017).
60. M. Zhou , Z. Liu , N. F. Loureiro , Intermittency and electron heating in kinetic-Alfvén-wave turbulence. arXiv [Preprint] (2022). http://arxiv.org/abs/2208.02441 (Accessed 4 August 2022).
61. G. G. Howes, A. J. McCubbin, K. G. Klein, Spatially localized particle energization by Landau damping in current sheets produced by strong Alfvén wave collisions. *J. Plasma Phys.* **84** (2018).
62. K. G. Klein, G. G. Howes, Measuring collisionless damping in heliospheric plasmas using field-particle correlations. *Astrophys. J. Lett.* **826**, L30 (2016).
63. G. G. Howes, K. G. Klein, T. C. Li, Diagnosing collisionless energy transfer using field-particle correlations: Vlasov–Poisson plasmas. *J. Plasma Phys.* **83**, 705830102 (2017).
64. N. F. Loureiro, A. A. Schekochihin, A. Zocco, Fast collisionless reconnection and electron heating in strongly magnetized plasmas. *Phys. Rev. Lett.* **111**, 025002 (2013).
65. R. Numata, N. F. Loureiro, Ion and electron heating during magnetic reconnection in weakly collisional plasmas. *J. Plasma Phys.* **81**, 305810201 (2015).
66. A. Kanekar, A. A. Schekochihin, W. Dorland, N. F. Loureiro, Fluctuation-dissipation relations for a plasma-kinetic Langevin equation. *J. Plasma Phys.* **81**, 305810104 (2015).
67. N. F. Loureiro *et al*., Viriato: A Fourier–Hermite spectral code for strongly magnetized fluid-kinetic plasma dynamics. *Comput. Phys. Commun.* **206**, 45–63 (2016).
68. N. F. Loureiro, A. A. Schekochihin, S. C. Cowley, Instability of current sheets and formation of plasmoid chains. *Phys. Plasmas* **14**, 100703 (2007).
69. G. G. Howes *et al*., Kinetic simulations of magnetized turbulence in astrophysical plasmas. *Phys. Rev. Lett.* **100**, 065004 (2008).
70. G. G. Howes, J. M. Tenbarge, W. Dorland, A weakened cascade model for turbulence in astrophysical plasmas. *Phys. Plasmas* **18**, 102305 (2011).
71. J. M. TenBarge, G. G. Howes, W. Dorland, Collisionless damping at electron scales in solar wind turbulence. *Astrophys. J.* **774**, 139 (2013).
72. J. M. TenBarge, G. G. Howes, Current sheets and collisionless damping in kinetic plasma turbulence. *Astrophys. J. Lett.* **771**, L27 (2013).
73. J. J. Podesta, J. E. Borovsky, S. P. Gary, A kinetic Alfvén wave cascade subject to collisionless damping cannot reach electron scales in the solar wind at 1 au. *Astrophys. J.* **712**, 685 (2010).
74. G. G. Howes, A prescription for the turbulent heating of astrophysical plasmas. *Mon. Not. R. Astron. Soc.: Lett.* **409**, L104–L108 (2010).
75. T. Passot, P. L. Sulem, A model for the non-universal power law of the solar wind sub-ion-scale magnetic spectrum. *Astrophys. J. Lett.* **812**, L37 (2015).
76. M. W. Kunz, I. G. Abel, K. G. Klein, A. A. Schekochihin, Astrophysical gyrokinetics: Turbulence in pressure-anisotropic plasmas at ion scales and beyond. *J. Plasma Phys.* **84**, 715840201 (2018).
77. A. J. McCubbin, G. G. Howes, J. M. TenBarge, Characterizing velocity–space signatures of electron energization in large-guide-field collisionless magnetic reconnection. *Phys. Plasmas* **29**, 052105 (2022).
78. V. Carbone, D. Telloni, F. Lepreti, A. Vecchio, High-frequency magnetic fluctuations in space plasmas and the role of electron Landau damping. *Astrophys. J. Lett.* **924**, L26 (2022).
79. G. W. Hammett, F. W. Perkins, Fluid moment models for Landau damping with application to the ion-temperature-gradient instability. *Phys. Rev. Lett.* **64**, 3019–3022 (1990).
80. C. K. Goertz, R. W. Boswell, Magnetosphere–ionosphere coupling. *J. Geophys. Res.: Space Phys.* **84**, 7239–7246 (1979).
81. A. Kumari, R. P. Sharma, N. Yadav, Inertial Alfvén wave induced turbulent spectra in aurora. *Astrophys. Space Sci.* **351**, 81–86 (2014).
82. M. J. Aschwanden, A. I. Poland, D. M. Rabin, The new solar corona. *Annu. Rev. Astron. Astrophys.* **39**, 175–210 (2001).
83. C. W. Smith, D. J. Mullan, N. F. Ness, R. M. Skoug, J. Steinberg, Day the solar wind almost disappeared: Magnetic field fluctuations, wave refraction and dissipation. *J. Geophys. Res.: Space Phys.* **106**, 18625–18634 (2001).
84. S. R. Cranmer, Coronal holes. *Living Rev. Solar Phys.* **6**, 1–66 (2009).
85. C. H. K. Chen, S. Boldyrev, Nature of kinetic scale turbulence in the Earth's magnetosheath. *Astrophys. J.* **842**, 122 (2017).
86. S. A. Orszag, C. M. Tang, Small-scale structure of two-dimensional magnetohydrodynamic turbulence. *J. Fluid Mech.* **90**, 129–143 (1979).
87. W. H. Matthaeus *et al*., Intermittency, nonlinear dynamics and dissipation in the solar wind and astrophysical plasmas. *Philos. Trans. R. Soc. A: Math. Phys. Eng. Sci.* **373**, 20140154 (2015).
88. Y. Kawazura, M. Barnes, A. A. Schekochihin, Thermal disequilibration of ions and electrons by collisionless plasma turbulence. *Proc. Natl. Acad. Sci. U.S.A.* **116**, 771–776 (2019).
89. V. Zhdankin, D. A. Uzdensky, G. R. Werner, M. C. Begelman, Electron and ion energization in relativistic plasma turbulence. *Phys. Rev. Lett.* **122**, 055101 (2019).
90. L. Arzamasskiy, M. W. Kunz, J. Squire, E. Quataert, A. A. Schekochihin, Kinetic turbulence in collisionless high-$\beta$ plasmas. *Phys. Rev. X* **13**, 021014 (2023).
91. R. Meyrand, J. Squire, A. A. Schekochihin, W. Dorland, On the violation of the zeroth law of turbulence in space plasmas. *J. Plasma Phys.* **87**, 535870301 (2021).
92. J. Squire *et al*., High-frequency heating of the solar wind triggered by low-frequency turbulence. *Nat. Astron.* **6**, 715–723 (2022).
93. M. Zhou , Z. Liu , N. F. Loureiro , Replication data for: Electron heating in kinetic-Alfvén-wave turbulence. Zenodo. https://doi.org/10.5281/zenodo.7789881. Deposited 31 March 2023.